LA-6773-PR

Progress Report

AFATL-TR-76-154

Special Distribution

Issued: April 1977

The Feasibility of Using Amatex in Air Force Submunitions

1 April—30 September 1976

G. F. Lederman, Jr., Capt. USAF

Work performed by:

A. W. Campbell
B. G. Craig
R. P. Engelke
G. F. Lederman, Jr., Capt. USAF
A. Popolato
T. Rivera

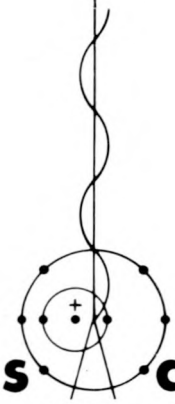

los alamos
scientific laboratory
of the University of California
LOS ALAMOS, NEW MEXICO 87545

An Affirmative Action/Equal Opportunity Employer

UNITED STATES
ENERGY RESEARCH AND DEVELOPMENT ADMINISTRATION
CONTRACT W-7405-ENG. 36

Previous reports in this series, unclassified, are LA-5992-PR and LA-6598-PR.

This work was performed for the Air Force Armament Laboratory with funds provided under Project Orders 5-0650-176 and ATL-6-0056. Larry Elkins, AFATL/DLDE, served as the Air Force project manager.

THE FEASIBILITY OF USING AMATEX IN AIR FORCE SUBMUNITIONS

1 April — 30 September 1976

by

G. F. Lederman, Jr., Captain, USAF

Work Performed by:

A. W. Campbell
B. G. Craig
R. P. Engelke
G. F. Lederman, Jr., Captain, USAF
A. Popolato
T. Rivera

I. SUMMARY

A. Initiation in Unconfined Submunition Configurations (Amatex/30 fill)

Unconfined BLU-61A/B and BLU-63/B submunitions were test-fired with standard (1.5 g) and oversize (3.0 g) RDX booster pellets. Only the BLU-61A/B with the oversize booster pellet sustained a detonation wave around its entire periphery. This wave was unidirectional, instead of proceeding symmetrically from the surface point of detonation breakout.

B. Effect of Diameter on Detonation Velocity

The detonation velocity of Amatex/30 was measured at five diameters, from 102 mm down to 10 mm. The detonation velocity varied from 7.275 mm/μs for 102-mm diam (corrected to ρ = 1.645 Mg/m^3) to 6.997 mm/μs for 19-mm diam (corrected to ρ = 1.645 Mg/m^3). A detonation was not sustained in the 10-mm-diam charge.

C. Shock Sensitivity

The shock sensitivity of Amatex/30 was measured in a series of wedge experiments. The shock sensitivity, expressed as the input pressure P_0 (GPa), that will result in a run of X*(mm) in the explosive before a high-order detonation begins, is log P_0 = 1.5543 − 0.7918 log X*.

D. Other

The effect of AN particle size on the detonation velocity of various Amatex formulations and shock sensitivity data for Amatex/20 are discussed in Appendixes A and B. The data contained in the Appendixes were obtained with a combination of DARPA, AFATL, and ERDA funds. They are included because most of the data are not generally available and they have some relevance to the objective of this study.

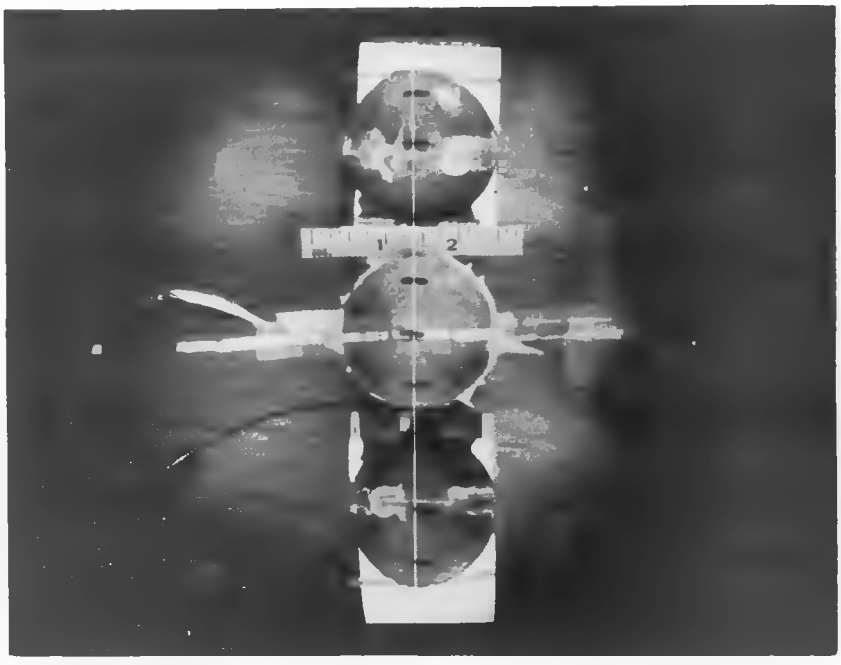

Fig. 1.
Still photograph of bare explosive charge for the BLU-63/B (E-3984). The middle image is a view directly parallel to the axis through the cylindrical axis of the inert fuze. The views on the other side are obtained from mirrors mounted at 45°. The top of the sphere is at the center of the photograph in the direct view and at the extreme edges in the mirror views. The black marks define the 45° positions around the charge. The white line across all the images is the smear camera slit image. The hemispherical joint can be seen in the two side views. The metal foils across the charge in the middle view form a pin switch.

II. INTRODUCTION

The objective of this study was to determine the feasibility of using Amatex in Air Force submunitions. Amatex is a castable mixture of ammonium nitrate (AN), RDX, and TNT. The amount of TNT is fixed at 40 wt%. The per cent of RDX is denoted by the number following the word Amatex. The remainder of the mixture is AN. Amatex is being considered as an alternate fill, and could be used when capacities of the RDX-producing plants are insufficient to meet the military requirements. The utilization of Amatex as an alternate fill for selected high-use munitions could reduce the requirement for additional RDX production capability that would, during periods of low use, remain idle. Ideally, preferred fills, such as Composition B (Comp. B) or Cyclotol 70/30, are replaced with the alternate fill with a minimum perturbation in the manufacturing (loading) plant, munition effectiveness, and storage and handling procedures.

The goals of this portion of the feasibility study are to determine the explosive parameters of Amatex/30. Among these are performance in a submunition configuration, the diameter dependence of the detonation velocity, and shock sensitivity.

III. INITIATION IN UNCONFINED SUBMUNITION CONFIGURATIONS

The initiation of detonation in Amatex/30 and the ability of the detonation wave to spread was studied by observing the arrival of the detonations at the periphery of uncased submunitions. A smear camera and mirror arrangement, as shown in Fig. 1, were used to record the arrival times as a function of position.[1]

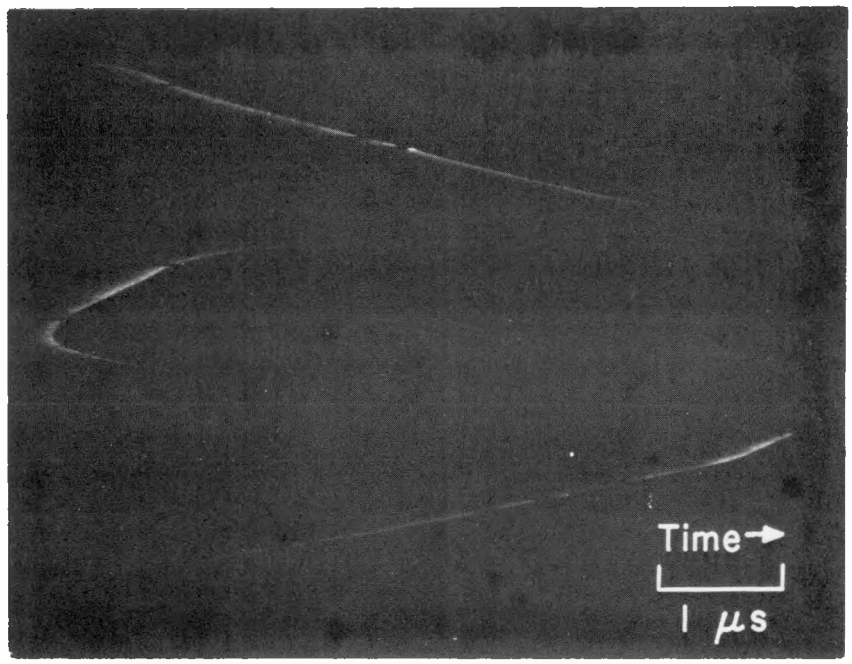

Fig. 2.
Wave trace for the bare BLU-63/B Comp. B charge (E-3984). The line in the photograph is the light from the detonation wave as it emerges from the surface of the sphere. The center record shows the wave emerging from the top hemisphere and sweeping in both directions around the charge. The traces at the sides are from the mirrors and show the wave from its emergence at the top until it sweeps around to the opposite hemisphere. The wave has the shape expected. Time increases to the right. The camera writing speed was 4.59 mm/μs.

Figure 2 shows a record obtained for a Composition B[1] (the preferred or standard fill for a BLU-63/B) charge. The detonation wave was high order and spread to intersect with the entire charge periphery. An RP-2 detonator was placed inside an inert fuze to initiate the explosive train (an RDX booster pellet which in turn initiates the main charge). Ionization pin switches were used to detect the arrival times on each side of the RDX booster and at a point on the periphery where the axis of the explosive train intersects the periphery.

The performance of Amatex/30 in four configurations (five shots) was studied with the above technique. The four configurations were:

(1) BLU-63/B, standard booster pellet (1.5 g, 14.9 mm diam, 5.21 mm high);
(2) BLU-63/B, oversize booster pellet (3.0 g, 21.7 mm diam, 5.21 mm high);
(3) BLU-61A/B, standard booster pellet (1.5 g, 14.9 mm diam, 5.21 mm high);
(4) BLU-61A/B, oversize booster pellet (3.0 g, 21.7 mm diam, 5.21 mm high).

Figures 3-6 show traces obtained with configurations 1-4, respectively.

Table I summarizes the measurements and inferences drawn from these experiments. It is concluded that, without substantial confinement, Amatex/30 explosive will not detonate in entirety except in configuration 4. Even in configuration 4, the detonation wave travels in one direction around the periphery instead of proceeding symmetrically from the point of initiation. This mode of initiation is the same as observed for Amatex/40 with a standard booster. An unconfined BLU-63/B Amatex/20 charge with a standard booster failed to propagate a detonation.[1]

IV. DETONATION VELOCITY AS A FUNCTION OF CHARGE DIAMETER FOR AMATEX/30

A. Test Procedure

The detonation velocity of Amatex/30 was measured on five rate sticks having diameters of 10, 19, 25, 51, and 102 mm. Each stick was boostered with TNT or Comp. B and a column of Amatex/30 of the same diameter as the rate-stick sections and at least six diameters long. The density was measured on each rate-stick section.

The rate sticks were assembled and fired as described in Ref. 2. The length of each element in a stick was measured to ± 3 μm, and the assembled stick was clamped together (total length equal to the sum of the elements).

The transit time of each stick section and of some of the booster sections was measured with ionization pin switches made of silver foil strips 3.2 mm wide and 12 μm thick. Two switches were inserted at each joint, and duplicate transit time measurements were taken. While the charge assemblies were on the firing mound, the temperature was held to 24 ± 1°C.

B. Results

Analysis was done by fitting the data to a linear, least squares equation. The resulting fit is D = 7.318 − 3.144 1/R, where D is the detonation velocity in mm/μs and R is the charge radius in mm. Table II gives the data, and Fig. 7 shows the data points fitted with the least squares equation. Failure diameter of Amatex/30 is between 10 and 19 mm. The infinite-diameter, detonation velocity is estimated to be 7.318 mm/μs. This compares with a value of 7.031 mm/μs obtained for Amatex/20.[3]

V. SHOCK SENSITIVITY OF AMATEX/30

Wedge experiments were performed[4] on Amatex/30 to determine its shock sensitivity. The charges used had densities of 1.650 ± 0.005 Mg/m³; the theoretical density is 1.719 Mg/m³ where the densities of RDX, AN, and TNT are, respectively, 1.801, 1.725, and 1.654 Mg/m³. Table III gives a summary of the experimental data, and Figs. 8 - 13 display the data in several formats.

Fig. 3.
Wave trace for the bare BLU-63/B Amatex/30 charge with the standard booster pellet (F-3968). The small amount of light visible is air shock, not detonation light. Detonation was not sustained.

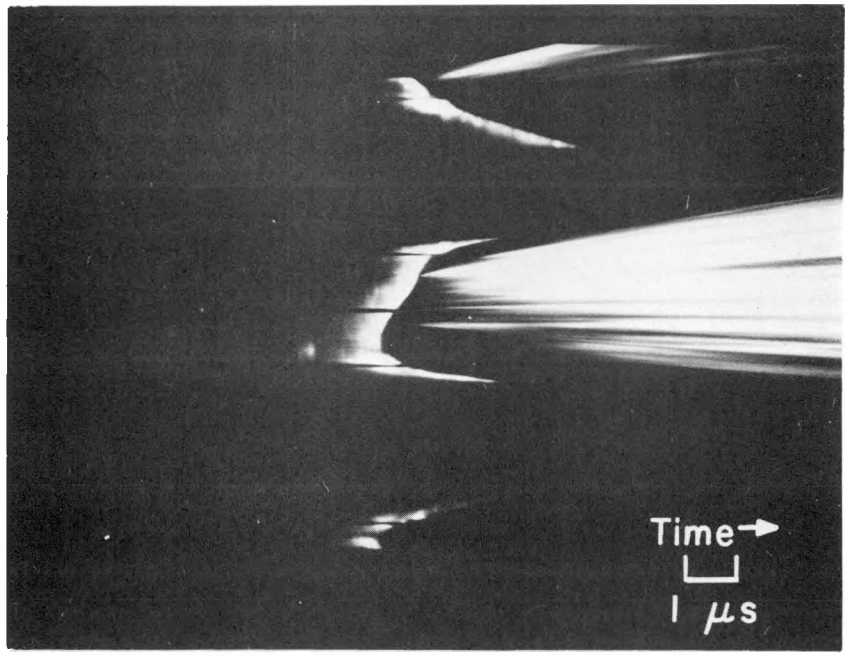

Fig. 4.
Wave trace for the bare BLU-63/B Amatex/30 charge with oversize booster pellet (E-4245). The detonation light is visible only to the submunition equator.

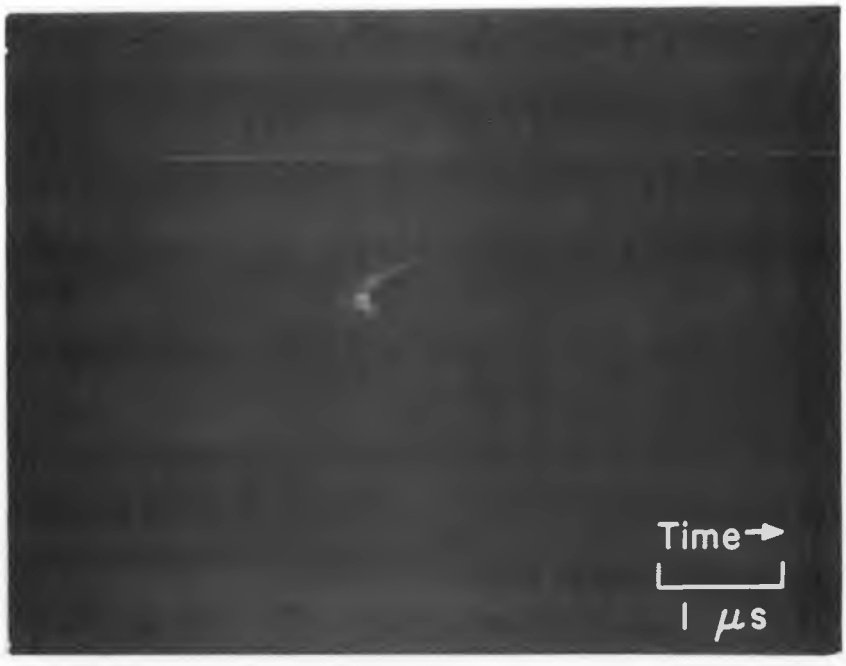

Fig. 5.
Wave trace for the bare BLU-61A/B Amatex/30 charge with standard booster pellet (F-3969). The small amount of light visible is air shock, not detonation light. Detonation was not sustained.

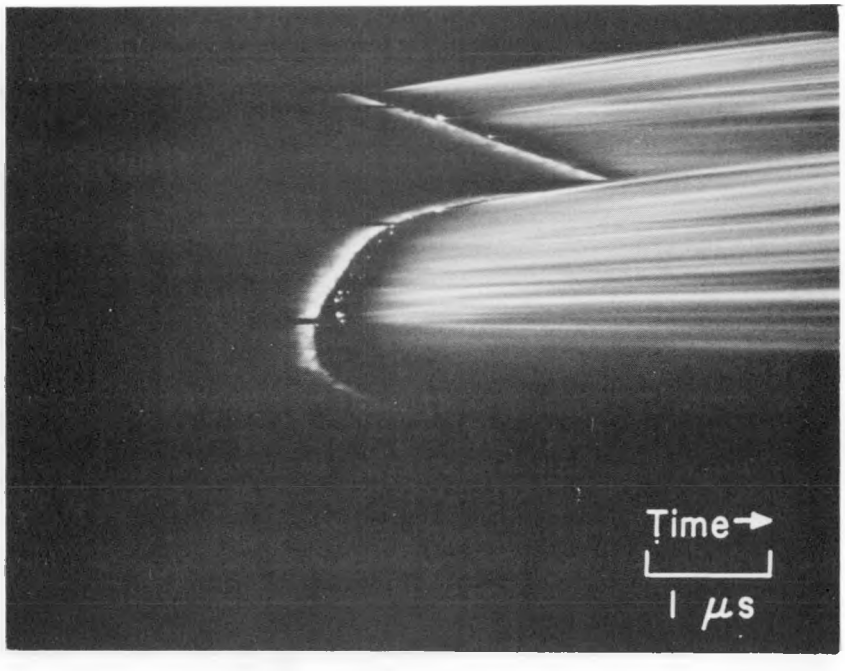

Fig. 6.
Wave trace for the bare BLU-61A/B Amatex/30 charge with the oversize booster pellet (F-3970). The detonation continued in one direction around the charge periphery and (not shown) eventually swept the entire circumference with the exception of the small, preshocked region above the booster pellet.

TABLE I

UNCASED BLU EXPERIMENT SUMMARY

Shot No.	Submunition	Booster Pellet	Time Through RDX Booster Pellet (μs)	TimeThrough Amatex/30 (μs)(Booster Pellet to Surface)	Results
F-3968	BLU-63/B	Standard	0.682	2.934	Detonation did not propagate.
F-3967	BLU-63/B	Oversize	0.67	2.04	No test.
E-4245	BLU-63/B	Oversize	No test	No test	Detonation sustained only to submunition equator.
F-3969	BLU-61A/B	Standard	No test	No test	Detonation did not propagate.
F-3970	BLU-61A/B	Oversize	0.662	3.934	Detonation sustained in one direction—swept around entire device, except for a small preshocked region near the initial breakout.

TABLE II

DIAMETER EFFECT FOR AMATEX/30

Shot No.	Amatex/30 Diameter (mm)	Composition Wt% TNT/RDX/AN	Density (Mg/m^3)	Equilibrium Velocity (mm/μs)	Equilibrium Velocity (mm/μs) Adjusted to ρ = 1.645 (Mg/m^3)[a]
E-4256	102	37.47/31.38/31.25	1.646	7.278	7.275
E-4255	51	37.52/30.08/32.40	1.649	7.185	7.173
E-4254	25	40.05/31.21/28.74	1.636	7.032	7.059
E-4290	19	37.90/30.82/31.28	1.645	6.997	6.997
E-4290	10	37.90/30.82/31.28	1.648	Detonation not sustained	

[a] $\Delta D = 3\frac{\text{mm}/\mu\text{s}}{\text{Mg/m}^3}\Delta\rho$, where ΔD is in mm/μs and $\Delta\rho$ is in Mg/m^3.

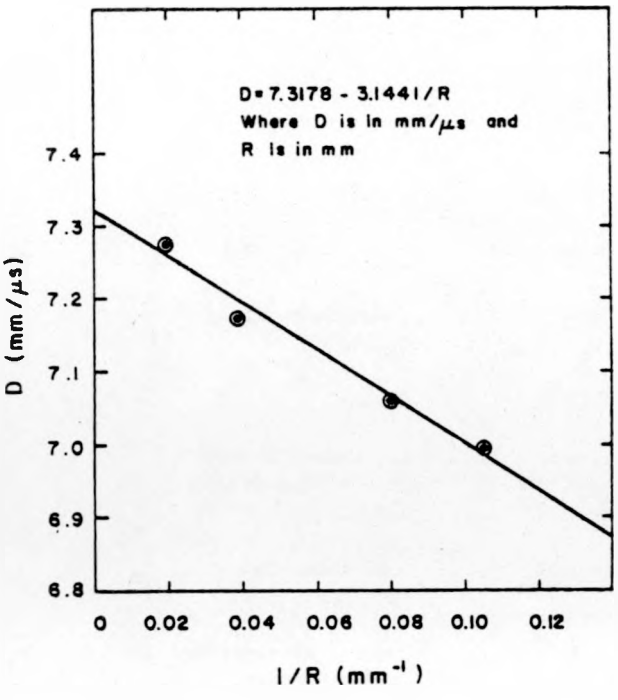

Fig. 7.
Diameter effect results for Amatex/30.

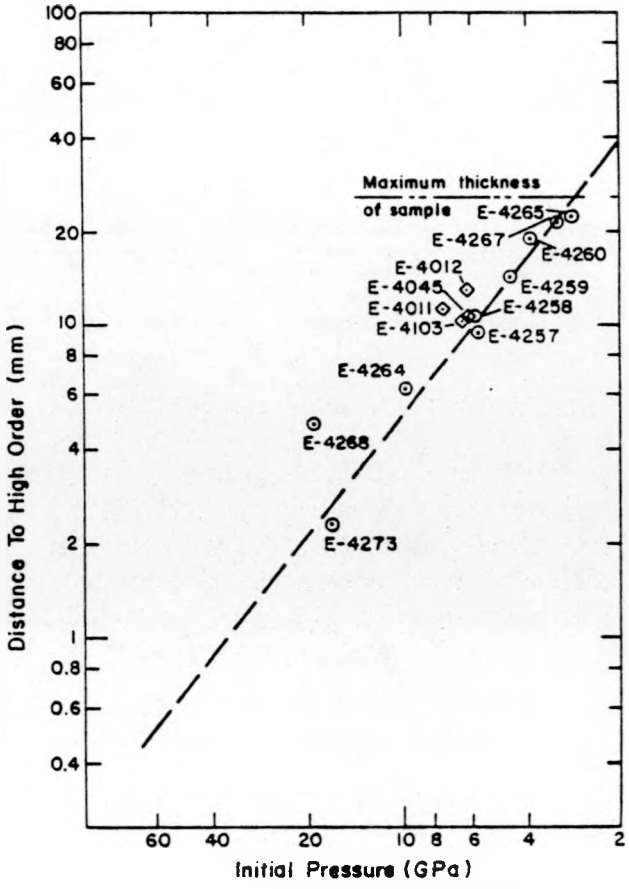

Fig. 8.
Plot showing the shock sensitivity of Amatex/30, ⊙, (ρ_0 = 1.650 Mg/m³). Dashed line is the least squares fit to the data: log P_0 = 1.5543-0.7918 log x^* where P_0 is in GPa and x^* is in mm. Shot E-4268 was cast out for the least squares fit. Data for Amatex/20, ◈, (ρ_0 = 1.582 Mg/m³) made with AN prills are also plotted for comparison (see Appendix B).

TABLE III

SUMMARY OF WEDGE DATA FOR AMATEX/30

ρ_0 = 1.650 Mg/m³, T_0 = 25°C

		Initial Shock Parameters			Coordinates For High Order		
Shot No.	P_0 (GPa)	U_{so}[a] (mm/μs)	U_p (mm/μs)	1/2b[a] (mm/μs²)	x* (mm)	t* (μs)	Driving System[b] (all thicknesses in mm)
E-4273	16.04	6.15	1.62	---	2.03	0.38	A, 6.38 Plexiglass
E-4268	18.08	6.685	1.717	0.182	4.88	0.72	B, 12.7 Plexiglas
E-4264	9.65	4.915	1.190	0.352	6.19	1.14	B, 48.9 Plexiglas
E-4257	6.70	4.116	0.989	0.447	9.35	1.84	C, 38.1 Plexiglas
E-4258	5.75	3.995	0.875	0.470	10.56	2.09	C, 38.1 Plexiglas
E-4259	4.40	3.816	0.699	0.176	14.13	3.13	D, 12.7 Plexiglas
E-4260	3.70	3.773	0.596	0.015	18.65	4.55	C, 25.4 SS[c], 12.4 Plexiglas
E-4267	3.05	3.433	0.538	0.063	20.15	5.12	C, 25.4 SS, 23.7 Plexiglas
E-4265	2.80	3.312	0.513	0.513	22.02	5.54	C, 25.4 SS, 23.7 Plexiglas
E-4261	2.60	3.291	0.480	0.055	>25.05	6.64	C, 17.8 PE[d], 11.5 SS, 11 Plexiglas
E-4274	1.27	2.657	0.290	0.000	>>26.03	9.84	E, 25.2 SS, 24.0 Plexiglas

[a]Parameters from fit to x-t data; $x = U_{so} + 1/2\ bt^2$.
[b]A P-081, 25.4 mm TNT.
B P-081, 25.4 mm Composition B.
C P-081, 25.4 mm Baratol.
D P-081, 50.8 mm TNT.
E P-120, 25.4 mm Baratol.
[c]Stainless steel type 304.
[d]Polyethylene.

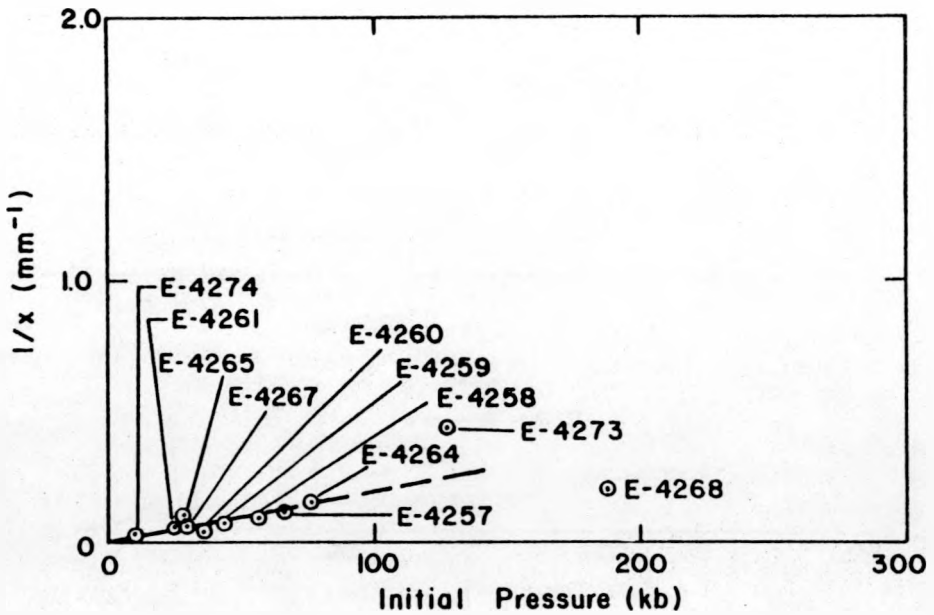

Fig. 9.
Plot showing the shock sensitivity of Amatex/30 (ρ_0 = 1.650 Mg/m³) in the 1/x vs P_0 plane.*

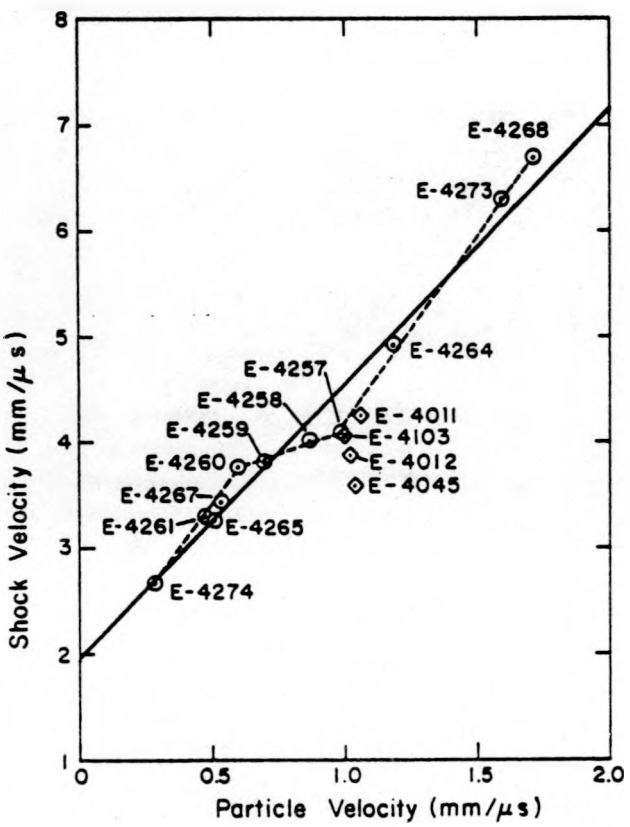

Fig. 10.
Shock Hugoniot for Amatex/30, ⊙, (ρ_0 = 1.650 Mg/m³). Solid line is the least squares fit to the data: U_s = 1.9479 + 2.5996 U_p, where U_s and U_p are in mm/μs. Note the data are fitted better with the 3 dashed lines. Such a fit suggests a phase change in the vicinity of 3.7-5.7 GPa. Data for Amatex/20, ◈ (see Appendix B), are also plotted but are inadequate to aid in determining the validity of a phase change.

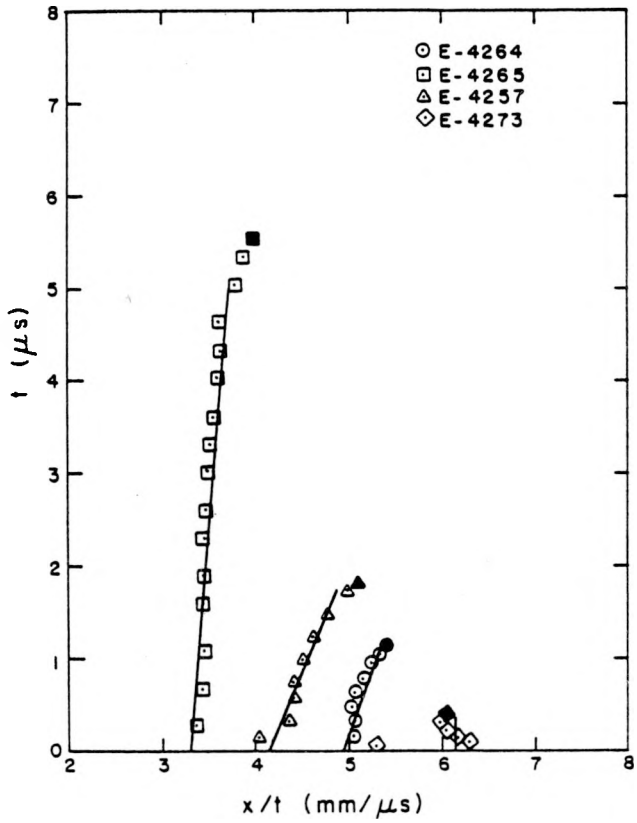

Fig. 11.
Plots of average shock velocity vs time for the low-order regime. Only representative data are plotted. Solid points represent the transition to high order.

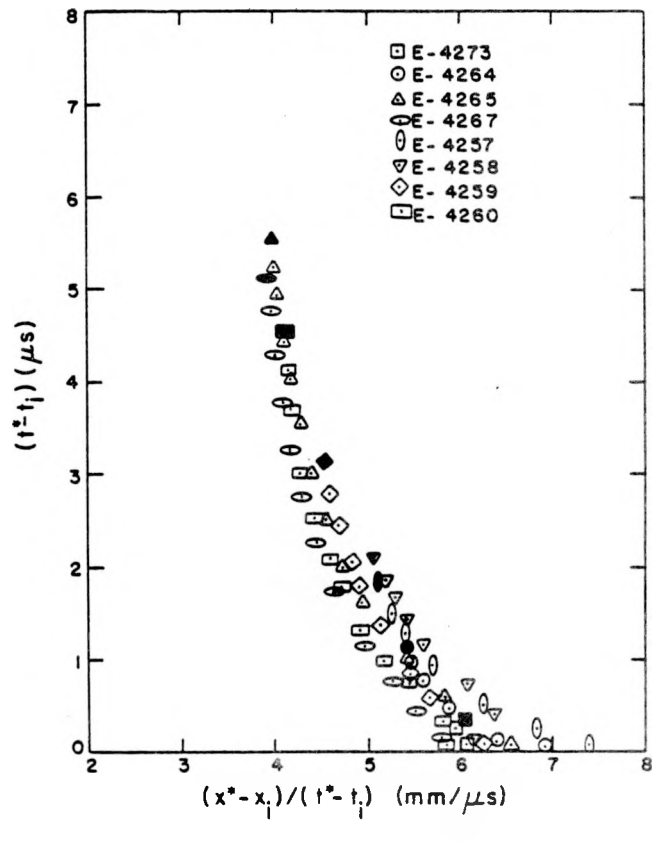

Fig. 12.
A test of the single-curve, build-up hypothesis for Amatex/30 (ρ_0 = 1.650 Mg/m³). Position ($x^* - x_i$) and time ($t^* - t_i$) were measured backward from the coordinates for transition to high-order detonation (x^*, t^*). Solid points are the time and velocity of the entering shockwave measured from the transition to high order.

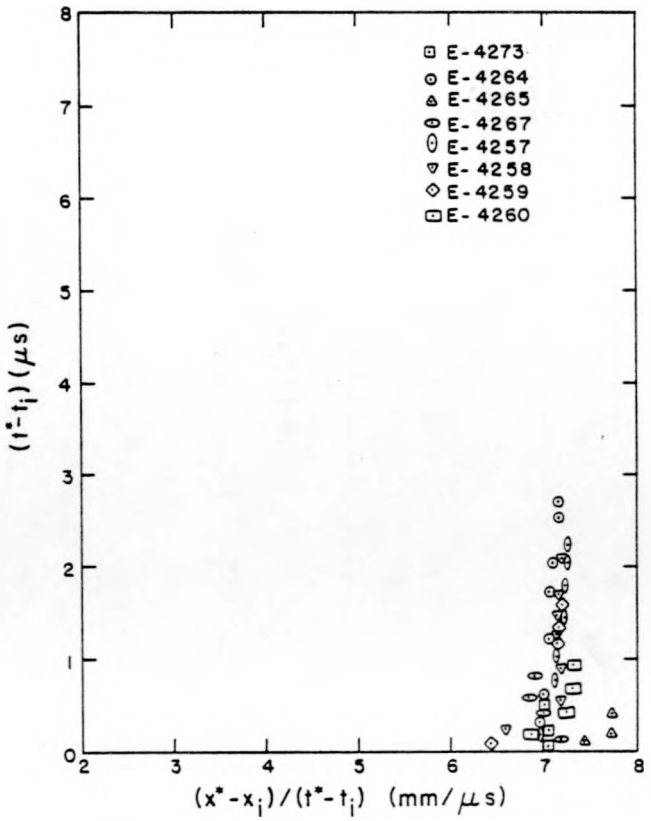

Fig. 13.
A plot of representative Amatex/30 (ρ_0 = 1.650 Mg/m³) data showing the phase velocity of the detonation wave after transition to high-order detonation. Transition occurs at $t_i - t^* = 0$ in this plane.

APPENDIX A

EFFECTS OF AMMONIUM NITRATE PARTICLE SIZE ON THE DETONATION BEHAVIOR OF AMATEX

I. INTRODUCTION

The following is a summary of detonation velocity tests and cylinder tests primarily on Amatex/20.

The question of interest is whether the AN particle size has a significant effect on performance. Important particle-size effects were observed in both detonation velocity and in the kinetic energy imparted to a cylinder wall.

II. EXPERIMENTAL

The cylinder tests were prepared and fired as described in Ref. 5, pp. 13-14. A smear-camera photograph of the expanding copper cylinder and a detonation-velocity measurement were made for each of the three small cylinders reported. Also, a plate dent was taken and an attempt was made to measure the cylinder fragment velocity by use of

two x-ray pictures obtained with portable x-ray equipment.

The reported detonation velocities of bare rate sticks were measured on precisely clamped assemblies.[2] All charges were temperature controlled to 24°C ± 2° and were initiated with small planewave lenses.

III. RESULTS

A. Cylinder Tests

Figure A-1 shows the relative efficiencies of Amatex explosives, prepared in various ways, for imparting kinetic energy to a confining metal casing (cylinder). The relative efficiency is expressed as a fraction of the kinetic energy imparted by a reference explosive at a corresponding expansion of the reference cylinder.

Curve I shows the reproducibility of precision cylinder tests for a duplicate pair of 25.4-mm-i.d. cylinders loaded with PBX-9404. For expansions greater than 4 mm, the reproducibility is better than 1.25%, and this precision may be imputed to the following curves.

Curve II is a comparison of data from a 25.4-mm-i.d. cylinder with scaled data from a 101.0-mm-i.d. cylinder, both loaded with Comp. B, Grade A (CB-GA). Here, "scaled" means that expansions for the larger cylinder have been divided by four for purposes of comparison. An important feature of this curve is that it shows that CB-GA fails to scale at late times by approximately 5%. This failure is contrary to the commonly held belief concerning scaling of high-performance explosives such as Comp. B and PBX-9404. Since the detonation velocity is not independent of diameter, some lack of scaling is to be expected.

Curves III and IV show two types of cast Amatex/20 compared to CB-GA, all fired in small cylinders (25.4 mm i.d.). Curve III is for Amatex/20 made with superfine AN (mean particle size of approximately 10 μm); Curve IV is for Amatex/20 standard grind (AN mean particle size of approximately 500 μm). From the curves, one sees that the superfine material is much more effective than the coarser material and that both materials are much less effective than CB-GA.

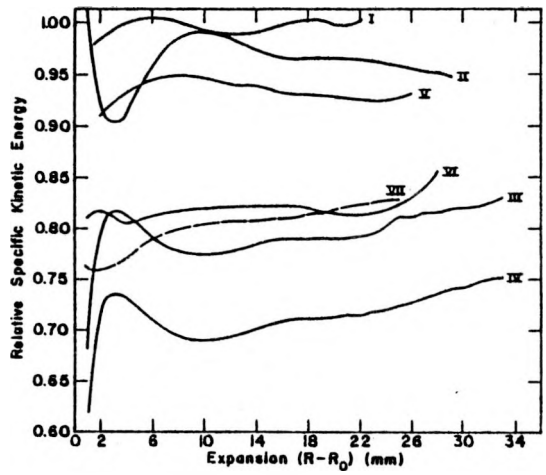

Fig. A-1.
Normalized, specific, kinetic-energy curves from cylinder tests.

All 101.0-mm cylinder expansions are scaled to equivalent 25.4-mm expansion.

Data for expansions less than 4 mm are of doubtful significance.

A horizontal line at relative energy = 1 would represent all experiments to which each of the following are normalized.

Key:

Curve I - Reproducibility from 25.4-mm cylinders containing PBX-9404. Shots C-4309 and C-4335.

Curve II - 25.4 mm CB-GA normalized to 101.0 mm CB-GA.

Curve III - 25.4 mm Amatex/20 (superfine) normalized to 25.4 mm CB-GA.

Curve IV - 25.4 mm Amatex/20 (standard grind) normalized to 25.4 mm CB-GA.

Curve V - 101.0 mm Amatex/40 (standard grind) normalized to 101.0 mm CB-GA.

Curve VI - 101.0 mm Amatex/20 (standard grind) normalized to 101.0 mm CB-GA.

Curve VII - 101.0 mm Amatex/20 (prilled) normalized to 101.0 mm CB-GA.

All 101.0-mm cylinder expansions are scaled to equivalent 25.4-mm expansion.

Curve V shows a comparison of Amatex/40 (standard grind) with CB-GA fired in large cylinders (101.0-mm i.d.). One notes that replacement of 20% of the RDX results in loss of only 7% in wall kinetic energy.

Curve VI shows a comparison of Amatex/20 (standard grind) with CB-GA fired in large cylinders (101.0-mm i.d.). A loss of approximately 17% in wall kinetic energy results from replacing 40% of the RDX in CB-GA.

Curve VII is a comparison of Amatex/20 made with prills (AN mean particle size of approximately 2000 μm) and CB-GA fired in large cylinders (101.0-mm i.d.). One notes, by comparison with Curve VI, that for mean particle sizes in the range 500 to 2000 μm there is an insignificant difference in the ability to drive the cylinder wall.

The results of these cylinder tests (Curves VI and VII) tend to agree with findings by Finger, et al.,[6] and Hershkowitz and Rigdon[7] that the energy imparted to a cylinder wall is independent of the oxidizer (AN) particle size until the size has been reduced to 5-10 μm (in *this* system size).

Scaling is more nearly realized for explosives (such as CB-GA) showing little diameter effect on the detonation velocity (see the following section). Curves III, VI, and VII, and the data in Table A-IV show that approximately the same energy is imparted to the cylinder wall by charges of the same composition (but of differing diameters and oxidizer particle sizes) if the detonation velocities are approximately equal. Nevertheless, the energy imparted to a cylinder wall cannot be simply related on a theoretical basis by the scaling factor (charge diameter ratio) and/or the initial pressure ratio ($\rho_1 D^2/\rho_2 D_2^2$).

Examples of reduced data are given in Tables A-I, A-II, and A-III for the three small cylinders.

B. Detonation Velocities

Figure A-2 is a collection of detonation-velocity data, corrected to density 1.615 Mg/m^3, for Amatex charges in which the diameter, confinement, and particle size have been varied.

Curve A is the diameter-effect curve for unconfined cast Amatex/20 standard grind (mean AN particle size of approximately 500 μm). The minimum diameter point on this curve is very close to the failure diameter. Curve B is the analogous result for the same material in copper confinement; the wall thickness is approximately one-tenth the charge diameter. The detonation velocities at the larger diameters are about as expected; the velocity at 1/R = 0.04 may be a little lower than its real value. The implied abrupt change in slope is unlikely. The smallest diameter charge shows a large confinement effect.

Curve C connects two points for the same material as that in Curve A except that the charges were pressed to shape rather than cast; both were fired unconfined. It was presumed that pressing would lead to smaller effective particle sizes for TNT and AN, and the data point at 1/R = 0.04 was expected to lie above the corresponding point on Curve A. Either the presumption is in error or the point at 1/R = 0.04 is anomalously low.

Curve D shows results for Amatex/20 made with superfine AN (mean particle size of approximately 10 μm), unconfined, and pressed to shape; Curve D lies above all the other curves for unconfined charges, as would be expected. Comparison with Curve G shows that the confinement effect is small for superfine material.

Curve E connects two points for cast, unconfined Amatex/20 made with prilled AN (mean particle size of approximately 2000 μm). This curve lies below all the other curves, as would be expected.

Curve A is typical of diameter-effect curves for solid explosives; one would expect the other curves to have a similar shape. Curve E, if fully developed, would appear to be consistent with Curve A. A comparison of these two curves suggests that there is a significant effect due to the AN particle-size change from 500 to 2000 μm at small charge diameters, although this effect is not significant in the 101-mm cylinder test. Curves B and C are anomalous—no explanation is accepted at present. The ordering of points among curves at any particular diameter is consistent with the expectation that smaller AN and TNT particle size would tend to result in higher detonation velocities.

A tabulation of all Amatex detonation velocities along with comparative data for CB-GA is given in Table A-IV.

TABLE A-I

COMPOSITION-B GRADE-A WALL EXPANSION DATA

Shot No. C-4430 Density = 1.696 Mg/m³; Loading Factor = 4.0331 Mg/m³

Expansion $(R - R_o)$(mm)	Time (μsec)	Calculated Wall Velocity (mm/μsec)	Calculated Wall Specific Kinetic Energy (mm/μsec)
1.[a]	1.106	0.974	0.949
2.[a]	2.074	1.092	1.192
3.[a]	2.950	1.190	1.416
4.[a]	3.763	1.268	1.608
5.	4.531	1.333	1.777
6.	5.267	1.384	1.915
7.	5.979	1.426	2.033
8.	6.671	1.459	2.129
9.	7.350	1.486	2.208
10.	8.018	1.507	2.271
11.	8.678	1.524	2.323
12.	9.331	1.538	2.365
13.	9.978	1.550	2.403
14.	10.62	1.560	2.434
15.	11.26	1.568	2.459
16.	11.90	1.576	2.484
17.	12.53	1.584	2.509
18.	13.16	1.591	2.531
19.	13.79	1.597	2.550
20.	14.41	1.604	2.573
21.	15.04	1.609	2.589
22.	15.66	1.614	2.605
23.	16.27	1.617[b]	2.615
24.	16.89	1.619	2.621
25.	17.51	1.621	2.628
26.	18.12	1.622	2.631
27.	18.74	1.624	2.637
28.	19.36	1.626	2.644
29.	19.97	1.627	2.647
30.	20.59	1.629	2.654
31.	21.20	1.631	2.660
32.	21.81	1.632	2.663
33.	22.42	1.634	2.670
33.7	22.85	1.635	2.673
asymptote[c]		$\approx$1.72	2.96

[a]Fluff obscured the wall, experimental data eliminated for $0 < t \leq 4.10$ μs [$0 < (R - R_o) \leq 4.73$ mm].
[b]Switch to quadratic fit at late times is made.
[c]Terminal velocity value obtained from x-ray records.

TABLE A-II

AMATEX/20 (STANDARD GRIND) WALL EXPANSION DATA

Shot No. C-4432 Density = 1.601 Mg/m³; Loading Factor = 4.0331 Mg/m³

Expansion $(R - R_0)$(mm)	Time (μsec)	Calculated Wall Velocity (mm/μsec)	$\frac{VEL^a}{VEL_{CB\text{-}GA}}$	$\left(\frac{VEL}{VEL_{CB\text{-}GA}}\right)^2$
1.	1.595	0.767	0.787	0.619
2.	2.772	0.923	0.845	0.714
3.	3.799	1.019	0.856	0.733
4.	4.748	1.084	0.855	0.731
5.	5.651	1.131	0.848	0.719
6.	6.521	1.166	0.842	0.709
7.	7.368	1.194	0.837	0.701
8.	8.198	1.216	0.833	0.694
9.	9.014	1.235	0.831	0.691
10.	9.818	1.252	0.831	0.691
11.	10.61	1.267	0.831	0.691
12.	11.40	1.281	0.833	0.694
13.	12.17	1.293	0.834	0.696
14.	12.94	1.304	0.836	0.699
15.	13.71	1.315	0.839	0.704
16.	14.47	1.324	0.840	0.706
17.	15.22	1.333	0.842	0.709
18.	15.97	1.340	0.842	0.709
19.	16.71	1.347	0.843	0.711
20.	17.45	1.353	0.844	0.712
21.	18.19	1.359	0.845	0.714
22.	18.92	1.364	0.845	0.714
23.	19.66	1.369	0.847	0.717
24.	20.38	1.374	0.849	0.721
25.	21.11	1.379[b]	0.850	0.723
26.	21.83	1.384	0.853	0.727
27.	22.55	1.389	0.855	0.731
28.	23.27	1.395	0.856	0.733
29.	23.99	1.399	0.860	0.740
30.	24.70	1.403	0.861	0.741
31.	25.41	1.407	0.863	0.745
32.	26.12	1.412	0.865	0.749
33.	26.83	1.416	0.867	0.751
34.	27.54	1.420		
34.8	28.10	1.424		
asymptote[c]		$\approx$ 1.44	0.839	0.704

[a]Composition B Grade A density 1.696 Mg/m³; $VEL_{CB\text{-}GA}$ wall velocity at equal expansion.
[b]Switch to quadratic fit at late times is made.
[c]Terminal velocity values obtained from x-ray record.

TABLE A-III

AMATEX/20 (SUPERFINE GRIND) WALL EXPANSION DATA

Shot No. C-4433 Density = 1.618 Mg/m³; Loading Factor = 4.0331 Mg/m³

Expansion $(R - R_0)$(mm)	Time (μsec)	Calculated Wall Velocity (mm/μsec)	$\frac{VEL^a}{VEL_{CB\text{-}GA}}$	$\left(\frac{VEL}{VEL_{CB\text{-}GA}}\right)^2$
1.	1.527	0.804	0.825	0.681
2.	2.648	0.971	0.889	0.791
3.	3.623	1.074	0.903	0.815
4.	4.524	1.143	0.901	0.813
5.	5.379	1.193	0.895	0.801
6.	6.204	1.231	0.889	0.791
7.	7.006	1.262	0.885	0.783
8.	7.791	1.286	0.881	0.777
9.	8.562	1.307	0.880	0.774
10.	9.321	1.326	0.880	0.774
11.	10.07	1.342	0.881	0.775
12.	10.81	1.356	0.882	0.777
13.	11.55	1.369	0.883	0.780
14.	12.27	1.380	0.885	0.783
15.	13.00	1.390	0.886	0.786
16.	13.71	1.399	0.888	0.788
17.	14.43	1.406	0.888	0.788
18.	15.14	1.413	0.888	0.788
19.	15.84	1.419	0.889	0.790
20.	16.55	1.425	0.888	0.788
21.	17.25	1.430	0.889	0.790
22.	17.94	1.436	0.890	0.792
23.	18.64	1.441	0.891	0.794
24.	19.33	1.448	0.894	0.800
25.	20.02	1.455[b]	0.899	0.809
26.	20.71	1.461	0.901	0.811
27.	21.39	1.465	0.902	0.814
28.	22.07	1.468	0.903	0.815
29.	22.74	1.472	0.905	0.819
30.	23.42	1.475	0.905	0.820
31.	24.09	1.479	0.907	0.822
32.	24.77	1.482	0.908	0.825
33.	25.45	1.486	0.911	0.830
34.	26.14	1.489		
34.2	26.26	1.490		
asymptote[c]		$\approx$ 1.52	0.882	0.778

[a]Composition B Grade A density 1.696 Mg/m³; $VEL_{CB\text{-}GA}$ wall velocity at equal expansion.
[b]Switch to quadratic fit at late times is made.
[c]Terminal velocity value obtained from x-ray records.

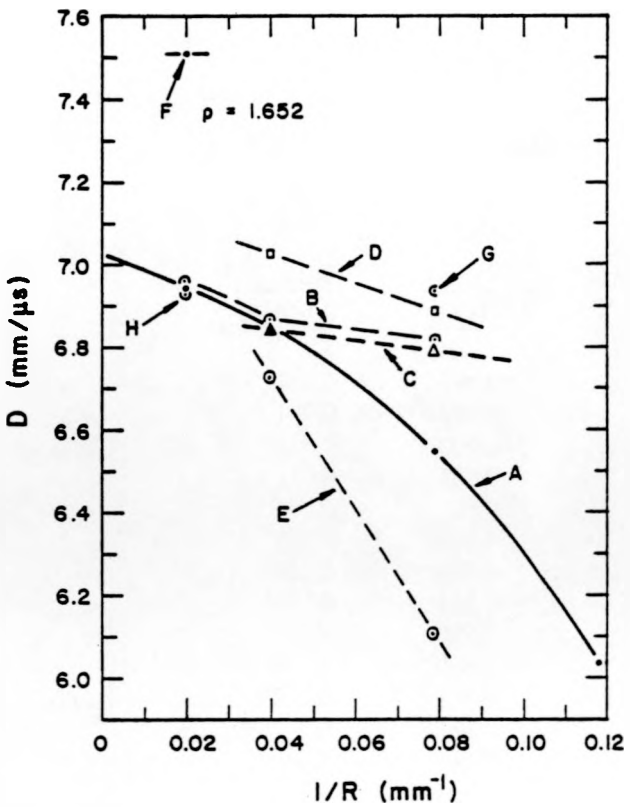

Fig. A-2.

Amatex diameter-effect curves for various diameters, confinements, and particle sizes. Curves A, B, C, D, and E are discussed in the text. Individual points F, G, H are identified in Table A-IV.

Key:

Rate Sticks:

- ● *Amatex/20 GR/C*
- △ *Amatex/20 GR/P*
- □ *Amatex/20 SF/P*
- ⊙ *Amatex/20 PR/C*

Cylinder Tests:

- ◔ *Amatex/20 SF/C*
- ◠ *Amatex/20 GR/C*
- ◡ *Amatex/20 PR/C*
- —●— *Amatex/40 GR/C*

PR ≡ prilled AN with mean particle size of approximately 2000 μm.

GR ≡ ground AN with mean particle size of approximately 500 μm.

SF ≡ superfine AN with mean particle size of approximately 10 μm.

C ≡ cast.

P ≡ pressed.

The diameter-effect curve for Amatex/20 standard grind, unconfined is $D(R) = D(\infty)\,[1 - A/(R - R_c)]$ *where,* $D(\infty) = 7.030 \pm 0.010$ *mm/μs,* $A = 0.585 \pm 0.031$ *mm, and* $R_c = 4.390 \pm 0.196$ *mm.*

TABLE A-IV

COLLECTION OF AMATEX DETONATION VELOCITIES

Shot No.	Explosive	Diam (mm)	Detonation Velocity (mm/μsec)	Density (Mg/m^3)	Confinement (mm OFHC copper) ρ = 8.920 Mg/m^3	Curve on Fig. A-2	Detonation Velocity Corrected to ρ = 1.615 Mg/m^3
E-3983	Amatex/20 GR/C	17.0	6.030	1.614	None	A	6.033
E-3817	Amatex/20 GR/C	25.4	6.542 ± 0.001	1.616	None	A	6.539
E-3819	Amatex/20 GR/C	50.8	6.833 ± 0.001	1.611	None	A	6.845
E-3823	Amatex/20 GR/C	101.6	6.937 ± 0.002	1.613	None	A	6.943
E-3999	Amatex/20 GR/P	25.4	6.804 ± 0.001	1.620	None	C	6.789
E-3998	Amatex/20 GR/P	50.8	6.845 ± 0.003	1.615	None	C	6.845
E-4007	Amatex/20 SF/P	25.4	6.905 ± 0.002	1.620	None	D	6.890
E-4006	Amatex/20 SF/P	50.8	7.023 ± 0.001	1.613	None	D	7.029
E-4033	Amatex/20 PR/C	25.4	6.143 ± 0.006	1.627	None	E	6.107
E-4034	Amatex/20 PR/C	50.8	6.766 ± 0.003	1.628	None	E	6.727
C-4317	Amatex/20 GR/C	50.8	6.857 ± 0.002	1.613	5.20	B	6.863
C-4321	Amatex/20 GR/C	101.0	6.951 ± 0.001	1.613	10.35	B	6.957
C-4397	Amatex/20 PR/C	101.0	6.805 ± 0.003	1.572	10.35	H	6.934
C-4389	Amatex/40 GR/C	101.0	7.510 ± 0.001	1.652	10.35	F	7.399
C-4374	Composition B Grade A/C	101.0	7.915 ± 0.002	1.701	10.35		7.657
C-4430	Composition B Grade A/C	25.4	7.867 ± 0.007	1.696	2.60		7.624
C-4432	Amatex/20 GR/C	25.4	6.810 ± 0.004	1.601	2.60	B	6.852
C-4433	Amatex/20 SF/P	25.4	6.941 ± 0.004	1.618	2.50	G	6.932

PR = Prilled ammonium nitrate (AN) with mean particle size of approximately 2000 μm.
GR = Ground AN with mean particle size of approximately 500 μm.
SF = Superfine AN with mean particle size of approximately 10 μm.
C = Cast.
P = Pressed.
†$\Delta D = 3\Delta\rho$ (mm/μsec) where $\Delta\rho$ is in units of Mg/m^3.

APPENDIX B

SHOCK SENSITIVITY OF AMATEX/20 (AN PRILLS)

A limited number of wedge experiments were performed with Amatex/20 prepared with prills of AN (mean particle size of approximately 2000 μm). The charges used had a density of 1.582 ± 0.002 Mg/m^3. Table B-I is a summary of the experimental data. Figures B-1 through B-3 display the data in several formats. The P-x* and U_s - U_p data are plotted in Figs. 8 and 10 (see main text), respectively.

TABLE B-1

SUMMARY OF WEDGE DATA FOR AMATEX/20 (PRILLED AN)

ρ_0 = 1.582 Mg/m³, T_0 = 25°C

	Initial Shock Parameters				Coordinates For High Order		
Shot No.	P_0 (GPa)	U_{so}[a] (mm/μs)	U_p (mm/μs)	$1/2b^2$ [a] (mm/μs²)	x* (mm)	t* (μs)	Driving System[b] (mm)
E-4104	2.75	2.961	0.587	0.052	>25.5	>7.41	A, 17.8 Polyethylene 11.5 SS[c], 11.0 Plexiglas
E-4046	2.78	2.886	0.609	0.102	>25.5	>6.95	A, 17.8 Plexiglas, 11.5 SS, 11.2 Plexiglas
E-4012	6.32	3.903	1.023	0.417	13.44	2.67	B, 46.4 Plexiglas
E-4103	6.48	4.061	1.009	0.339	10.31	2.18	A, 38.1 Plexiglas
E-4045	6.25	3.606	1.096	0.433	11.07	2.38	A, 38.6 Plexiglas
E-4011	7.48	4.237	1.116	0.287	11.43	2.33	A, 22.4 Plexiglas

[a]Parameters from fit to x − t data: $x = U_{so} + 1/2bt^3$.
[b]A. P-081, 25.4 mm Baratol
B. P-081, 38.1 mm Baratol
[c]Type 304 stainless steel.

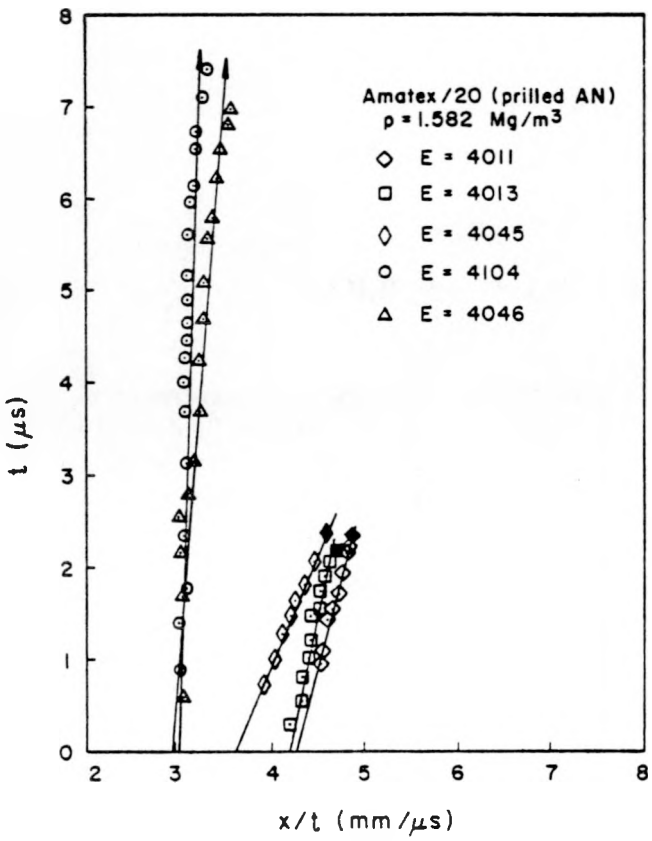

Fig. B-1.
Plots of average shock velocity vs time for the low-order regime of Amatex/20 (AN prills). Only representative data are plotted. Solid points represent the transition to high order.

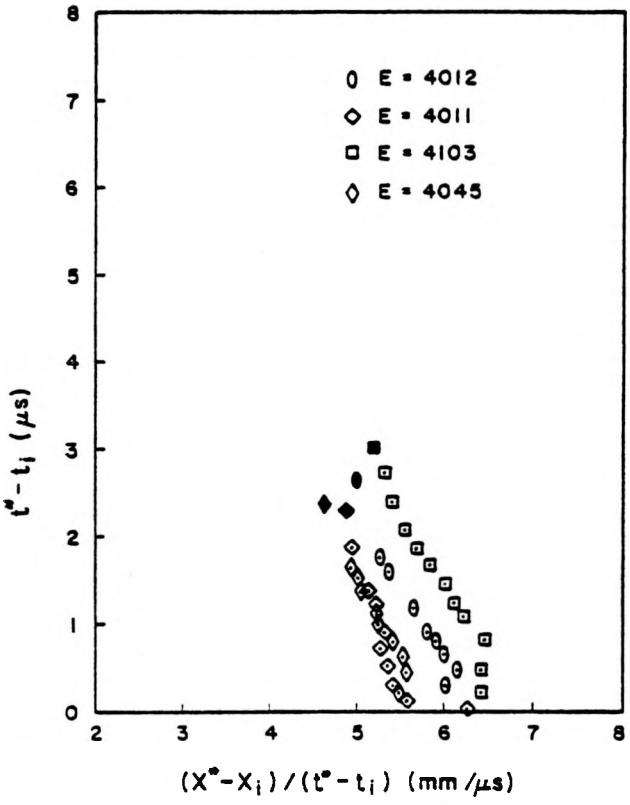

Fig. B-2.

A test of the single-curve build-up hypothesis for Amatex/20 (AN prills). Position ($x^* - x_i$) and time ($t^* - t_i$) were measured backward from the coordinates for transition to high-order detonation (x^*, t^*). Solid points are the time and velocity of the entering shock wave measured from the transit to high order. The scatter is unusually large, presumably due to the quality of a charge cast with AN prills.

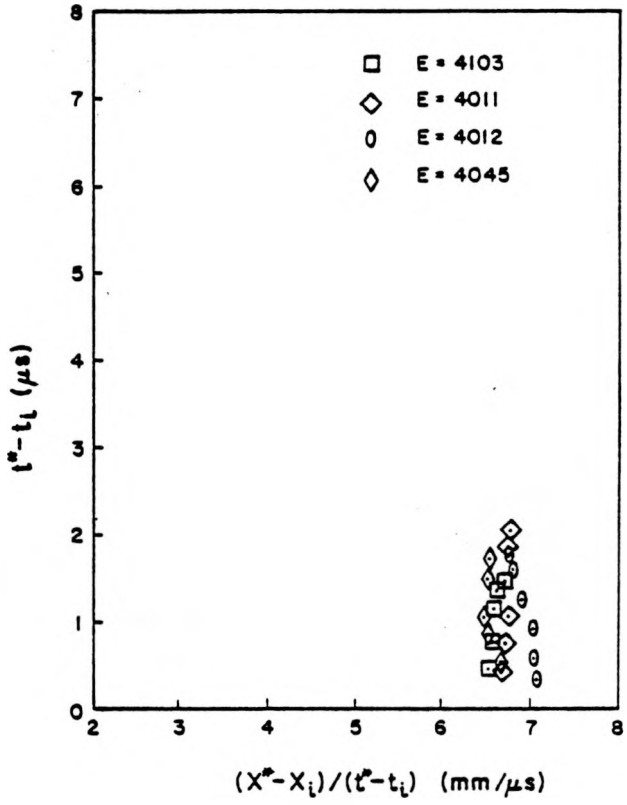

Fig. B-3.

A plot of representative Amatex/20 (AN prills) data showing the phase velocity of the detonation wave after transition to high-order detonation. Transition occurs at $t^* - t_i = 0$ in this plane. The scatter is due to nonuniformities in the charges that resulted in nonsimultaneous initiation and tilted detonation waves.

REFERENCES

1. A. Popolato, "The Feasibility of Using Amatex in Air Force Submunitions, February 15—November 30, 1974," Los Alamos Scientific Laboratory Report LA-5992-PR and AFATL TR-75-56 (1975).

2. A. W. Campbell, M. E. Malin, T. J. Boyd, Jr., and J. A. Hull, "Precision Measurement of Detonation Velocities in Liquid and Solid Explosives," Rev. Sci. Instr. **27**, 567-574 (1956).

3. A. Popolato, A. W. Campbell, L. W. Hantel, H. R. Lewis, P. G. Salgado, and B. G. Craig, "Properties of Amatex/20," Los Alamos Scientific Laboratory Report LA-5516-MS (March 1974).

4. A. W. Campbell, W. C. Davis, J. B. Ramsay, and J. R. Travis, "The Shock Initiation of Solid Explosives," Physics of Fluids **4**, 511 (1961).

5. A. Popolato, "Quarterly Report Joint Services Explosive Program," Los Alamos Scientific Laboratory Report LA-5711-PR (August 1974).

6. M. Finger, H. C. Hornig, E. L. Lee, and J. W. Kury, "Metal Acceleration By Composite Explosives," Fifth Symposium on Detonation, Pasadena, California (1970).

7. J. Hershkowitz and J. Rigdon, "Evaluation by a Modified Cylinder Test of Metal Acceleration by Non-Ideal Explosives Containing Ammonium Nitrate," Picatinny Arsenal Technical Report 4611 (1974).

SPECIAL DISTRIBUTION

	No. of Copies
HQ USAF/RDQRM Washington, DC 20330	2
HQ USAF/SAMI Washington, DC 20330	1
AFSC/SDWM Andrews AFB Washington, DC 20331	1
AFSC/IGFG Andrews AFB Washington, DC 20331	1
HQ AFSC/DLCAW Andrews AFB Washington, DC 20331	1
AFLC/MMWmC Attn: H. Storer Wright-Patterson AFB, OH 45433	2
ASD/ENYEHM Wright-Patterson AFB, OH 45433	1
ASD/ENYS Wright-Patterson AFB, OH 45433	1
AFWL/LR Kirtland AFB, NM 87117	1
AFWL/SUL Kirtland AFB, NM 87115	1
AUL/AUL-LSE-70-239 Maxwell AFB, AL 36112	1
Ogden ALC/MMNOP Hill AFB, UT 84406	2
MMECB OOAMA Attn: Mr. Bailey Hill AFB, UT 84406	2
AEDC/ARO, Inc. Attn: Lib/DLCS Arnold AFS, TN 37389	1
AFATL/DL Eglin AFB, FL 32542	1
AFATL/DLY Eglin AFB, FL 32542	1
AFATL/DLOSL Eglin AFB, FL 32542	2
AFATL/DLYV Eglin AFB, FL 32542	1
AFATL/DLDE Eglin AFB, FL 32542	4
ADTC/WE Eglin AFB, FL 32542	1
AFATL/DLX Eglin AFB, FL 32542	1
TAWC/TRADOCLO Eglin AFB, FL 32542	1
Redstone Science Information Center Attn: Chief, DOC SEC USA Missile Command Redstone Arsenal, AL 35809	2
Director USA Material Systems Analysis Agency Attn: AMXSY-DS Aberdeen Proving Ground, MD 21005	1
Director USA Material Systems Analysis Agency Attn: AMXSY-DD Aberdeen Proving Ground, MD 21005	1
Director USA Material Systems Analysis Agency Attn: AMXSY-A Aberdeen Proving Ground, MD 21005	1
Ballistic Research Laboratories USA Aberdeen R&D Center Attn: AMXBR-TB Aberdeen Proving Ground, MD 21005	1
Commanding Officer Frankford Arsenal Attn: LIB, K2400, Bldg. 51-2 Philadelphia, PA 19137	1
Commander Picatinny Arsenal Attn: SARPA-FS, Bldg. 59 Dover, NJ 07801	1
Commander Picatinny Arsenal Attn: A. Loeb, SARPA-FR-S-A Dover, NJ 07801	1
Commander Picatinny Arsenal Attn: A. M. Anzalone, Plastec - Bldg. 17 Dover, NJ 07801	1
Commander Picatinny Arsenal Attn: Dr. R. F. Walker, SARPA-FRL Dover, NJ 07801	1
Commander Picatinny Arsenal Attn: Dr. H. J. Matsuguma, SARPA-FRL Dover, NJ 07801	1
Commander Picatinny Arsenal Attn: I. Akst, SARPA-FRL Dover, NJ 07801	1

	No. of Copies
Office of the Chief of Naval Operations Air Warfare Branch (OP-982E) Pentagon Building, Room 5C723 Washington, DC 20350	1
Commander US Army Materiel Command Attn: AMCRD-WN (Mr. Corrigan) Alexandria, VA 22304	1
Commanding Officer Watervliet Arsenal Attn: SARWV-RDT-L Watervliet, NY 12189	1
Director Naval Research Laboratory Attn: Code 2627 Washington, DC 20375	1
Commander Naval Surface Weapons Center Attn: J. Enig White Oak, Silver Spring, MD 20910	1
Commander Naval Surface Weapons Center Attn: H. Heller White Oak, Silver Spring, MD 20910	1
Commander Naval Surface Weapons Center Attn: J. Leahy White Oak, Silver Spring, MD 20910	1
Commander Naval Surface Weapons Center Attn: I. Kabik White Oak, Silver Spring, MD 20910	1
Commander Naval Surface Weapons Center Technical Library, Information White Oak, Silver Spring, MD 20910	2
Naval Ordnance Station Attn: Technical Library Indian Head, MD 20640	1
Commanding Officer Naval Weapons Station/20323 Yorktown, VA 23691	1
Commander, Code 533 Naval Weapons Center Attn: Technical Library China Lake, CA 93555	2
Commander, Code 51102 Naval Weapons Center Attn: Paul H. Miller China Lake, CA 93555	1
Commander, Code 4541 Naval Weapons Center Attn: C. D. Lind China Lake, CA 93555	1
Commander, Code 45401 Naval Weapons Center Attn: H. J. Gryting China Lake, CA 93555	1
Commander, Code 454 Naval Weapons Center Attn: R. Reed China Lake, CA 93555	1
Commander, Code 34336 Naval Weapons Center Attn: J. M. Pakulak, Jr. China Lake, CA 93555	1
Commander, Code 4565 Naval Weapons Center China Lake, CA 93555	1
Naval Air Systems Command Code AIR-5323 Washington, DC 20361	1
Office of Naval Research/Code 473 Attn: Ralph Roberts Arlington, VA 22217	1
Commander Naval Weapons Laboratory Dahlgren, VA 22448	1
Commander Naval Weapons Laboratory Attn: W. A. Kemper Dahlgren, VA 22448	1
Naval Weapons Evaluation Facility Code/WE Kirtland AFB Albuquerque, NM 87117	1
Naval Sea Systems Command Attn: A. Amster (SEA-0332) Washington, DC 20360	1
Naval Sea Systems Command Attn: R. Beauregard (SEA-992E) Washington, DC 20360	1
University of California Lawrence Livermore Laboratory Attn: J. W. Kury P. O. Box 808 Livermore, CA 94550	1
University of California Lawrence Livermore Laboratory Attn: E. Lee P. O. Box 808 Livermore, CA 94550	1
University of California Lawrence Livermore Laboratory Attn: H. F. Rizzo P. O. Box 808 Livermore, CA 94550	1

	No. of Copies
University of California Lawrence Livermore Laboratory Attn: F. E. Walker P. O. Box 808 Livermore, CA 94550	1
University of California Lawrence Livermore Laboratory Attn: M. Finger P. O. Box 808 Livermore, CA 94550	1
University of California Lawrence Livermore Laboratory Attn: R. McGuire P. O. Box 808 Livermore, CA 94550	1
University of California Lawrence Livermore Laboratory Attn: Chemistry Department/L-402 P. O. Box 808 Livermore, CA 94550	1
University of California Lawrence Livermore Laboratory Attn: Technical Information Department L-3 P. O. Box 808 Livermore, CA 94550	1
Chem Prop Info Agency Applied Physics Laboratory Johns Hopkins University 8621 Georgia Ave. Silver Spring, MD 20910	1
Battelle Memorial Institute Attn: Reports Library 505 King Ave. Columbus, OH 43201	1
DDC/TC Cameron Station Alexandria, VA 22314	2
Harry Diamond Laboratories Attn: AMXDP-TC Washington, DC 20438	1
AFIS (INTA) Washington, DC 20330	1
Mason & Hanger-Silas Mason Co., Inc. Pantex Plant Attn: Mail and Records For: G. T. West, R. J. Slape, J. A. Crutchmer, P. A. Foster, P. E. Kramer, J. H. VanVelkinburgh P. O. Box 647 Amarillo, TX 79177	6
Los Alamos Scientific Laboratory Attn: Report Library P. O. Box 1663 Los Alamos, NM 87544	1
U.S. Energy Research and Development Administration HQS Library, Room G-042 Washington, DC 20545	1